Solution Structure of a 2:1 C2-(2-Naphthyl) Pyrrolo[2,1-*c*][1,4]benzodiazepine DNA Adduct: Molecular Basis for Unexpectedly High DNA Helix Stabilization[†,‡]

Dyeison Antonow,[§,||] Teresa Barata,[⊥] Terence C. Jenkins,[#] Gary N. Parkinson,[⊥] Philip W. Howard,[§,||] David E. Thurston,*[,§,||] and Mire Zloh*[,⊥]

Gene Targeting Drug Design Research Group, Spirogen Ltd., and The School of Pharmacy, University of London, 29/39 Brunswick Square, London WC1N 1AX, U.K., and Morvus Technology Limited, Tŷ Myddfai, Llanarthne, Carmarthen SA32 8HZ, U.K.

Received June 30, 2008; Revised Manuscript Received August 9, 2008

ABSTRACT: The naturally occurring pyrrolo[2,1-*c*][1,4]benzodiazepine (PBD) monomers such as sibiromycin, anthramycin, and tomaymycin form stable covalent adducts with duplex DNA at purine−guanine−purine sites. A correlative relationship between DNA-binding affinity, as measured by enhanced thermal denaturation temperature of calf thymus DNA (T_m), and cytotoxicity is well documented for these naturally occurring compounds and a range of synthetic analogues with sibiromycin having the highest ΔT_m value (16.3 °C), reflecting favorable hydrogen-bonding interactions between the molecule and DNA bases. We report here that, surprisingly, the structurally simple synthetic C2-(2-naphthyl)-substituted pyrrolo[2,1-*c*][1,4]benzodiazepine monomer (**5**) has a ΔT_m value (15.8 °C) similar to that of sibiromycin and significantly higher than the values for either anthramycin (13.0 °C) or tomaymycin (2.6 °C). **5** also has similar cytotoxic potency to sibiromycin which is widely regarded as the most potent naturally occurring PBD monomer. To investigate this, we have used NMR in conjunction with molecular dynamics to study the 2:1 adduct formed between **5** and the DNA duplex d(AATCTTTAAAGATT)$_2$. In contrast to the hydrogen-bonding interactions which predominate in the case of sibiromycin and anthramycin adducts, we have shown that the high binding affinity of **5** is due predominantly to hydrophobic (van der Waals) interactions. The high-resolution 2D NOESY, TOCSY, and COSY data obtained have also allowed unequivocal determination of the orientation of the PBD molecule (A-ring toward 3′-end of covalently bound strand), the stereochemistry at the C11 position of the PBD (C11*S*), and the conformation of the C2-naphthyl ring which extends along the floor of the minor groove thus optimizing hydrophobic interactions with DNA. These results provide opportunities for future drug design in terms of extending planar hydrophobic groups at the C2 position of PBDs to maximize binding affinity.

The pyrrolo[2,1-*c*][1,4]benzodiazepines (PBDs)[1] are a family of natural products produced by *Streptomyces* species with the unique characteristic of forming nondistortive covalent adducts in the minor groove of DNA specifically at purine−guanine−purine sequences (*1*). For this reason there is interest in using PBDs as part of a small-molecule strategy for targeting DNA sequences (*2*) and also as novel anticancer (*3*) and antibacterial agents (*4*). Anthramycin (**1**) was the first PBD to be isolated and characterized, and its structure was confirmed by X-ray crystallography (*5, 6*). Since then, over ten other related compounds have been isolated from different *Streptomyces* species providing a diversity of structures based on the core pyrrolobenzodiazepine scaffold but distinguished from anthramycin by the type and position of substituents in the A- and C-rings and the degree and position of points of unsaturation in the C-ring. For example, sibiromycin (**2**) is characterized by the sibirominose sugar at the C8 position of the A-ring (*7, 8*), whereas anthramycin (**1**) and tomaymycin (**3**) differ in having either C2/C3-*endo* or C2-*exo* unsaturation (Figure 1).

The structure of PBD−DNA adducts has been the subject of many studies using methodologies including NMR (*9*−*11*), X-ray crystallography (*12*), molecular modeling (*13, 14*), DNA thermal denaturation (*15*), gel-based techniques (*16, 17*), and, more recently, mass spectrometry (*18*). These studies have established that PBDs bind covalently to the C2-NH$_2$

[†] This research was supported by Cancer Research UK (Grant C180/A1060 to D.E.T.), Spirogen Ltd., and the Engineering and Physical Sciences Research Council (GR/R47646/01).

[‡] Biological Magnetic Resonance Data Bank (BMRB) entry 15613; Protein Data Bank (PDB) entry 2k4l; Research Collaboratory for Structural Bioinformatics (RCSB) entry RCSB100668.

* Corresponding authors. E-mail: david.thurston@pharmacy.ac.uk; mire.zloh@pharmacy.ac.uk.

[§] Gene Targeting Drug Design Research Group, The School of Pharmacy, University of London.

[||] Spirogen Ltd., The School of Pharmacy, University of London.

[⊥] The School of Pharmacy, University of London.

[#] Morvus Technology Limited.

[1] Abbreviations: COSY, correlated spectroscopy; CT-DNA, calf thymus DNA; ΔT_m, enhancement in thermal denaturation temperature of calf thymus DNA; DCM, dichloromethane; DMSO, dimethyl sulfoxide; DQF, double-quantum filtered; HPLC, high-performance liquid chromatography; NMR, nuclear magnetic resonance; NOE, nuclear Overhauser enhancement; 2D NOESY, two-dimensional nuclear Overhauser enhancement spectroscopy; PBD, pyrrolo[2,1-*c*][1,4]-benzodiazepine; Py, pyrimidine nucleotides; Pu, purine nucleotides; TOCSY, total correlation spectroscopy; TSP, 3-(trimethylsilyl)propionic acid-d_4 sodium salt; "×" (as in "H6−C4 × H5−C4"), a cross-peak between proton 6 and proton 5 of the 4th cytosine residue.

10.1021/bi801225q CCC: $40.75
Published on Web 10/17/2008

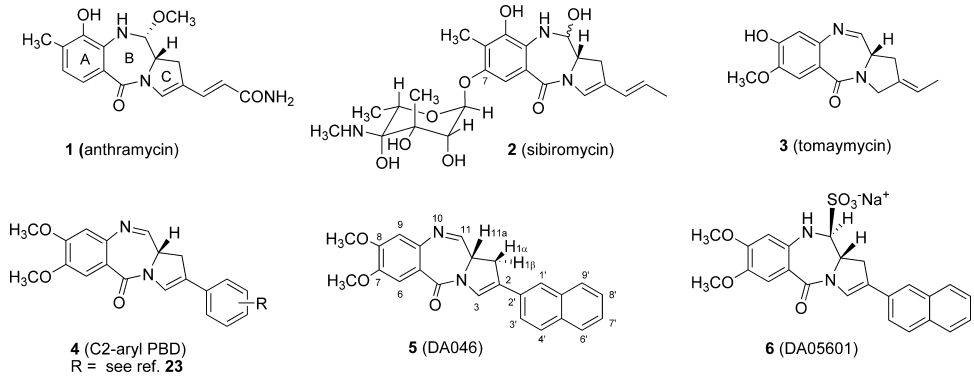

FIGURE 1: Top: Naturally occurring PBDs anthramycin (**1**), sibiromycin (**2**), and tomaymycin (**3**). Bottom: Synthetic C2-Aryl PBDs (**4**), the C2-naphthyl PBD (**5**), and its water-soluble C11 sodium bisulfite form (**6**).

position of guanine bases through their electrophilic N10-C11 imine functionality. Hydrogen bonds and hydrophobic interactions further stabilize the PBD molecule, allowing a snug fit in the minor groove with the A-ring orientated toward the 3′-end of the covalently modified strand. Combined, the covalent and additional noncovalent interactions, and the similarity in shape between the molecules and the minor groove twist encountered in Pu-G-Pu sequences (*12*), account for the preference for GGG or AGA binding sites, as observed in gel-based experiments such as DNA footprinting and *in vitro* transcription stop assays (*16, 17*).

The potential of the PBD scaffold for use in gene targeting and for producing novel anticancer and anti-infective agents has led to the synthesis of a wide range of both monomeric and dimeric PBD structures. One example of the latter, SJG-136, is showing promising activity in clinical trials (*3*). These new synthetic molecules have contributed significantly to the understanding of SARs for the PBD family. For example, recent chemical studies have established that, for both PBD monomers and dimers, C2/C3-*endo* unsaturation coupled with C2 substitution can substantially enhance cytotoxicity and DNA-binding affinity (*19, 20*). It has been shown that potency is enhanced still further if this C2 substituent is an aryl group. For example, Cooper and co-workers have demonstrated that analogues of this type (e.g., **4** in Figure 1) (*21*) are potently and selectively cytotoxic toward melanoma and renal cancer tumor cells within the 60 cell lines of the NCI panel, with some showing antitumor activity in relevant *in vivo* models (*22*). As a continuation of these studies we have carried out a parallel synthesis of a 66-membered library with structurally diverse C2-aryl substituents (*23*). One analogue containing a C2-naphthyl substituent (**5**) stood out from other library members in having an usually high affinity for double-stranded DNA as measured by thermal denaturation (i.e., $\Delta T_m = 15.8$ °C, compared to 16.3 °C for sibiromycin) and in being similarly potent to sibiromycin in terms of *in vitro* cytotoxicity.[2] This was intriguing given the relatively simple structure of **5**. It had been previously assumed (*24, 25*) that the C7-sugar moiety of sibiromycin contributed to it having the highest reported ΔT_m value for any PBD monomer, either naturally occurring or synthetic.

Therefore, we decided to use high-field NMR in conjunction with molecular dynamics to study a 2:1 adduct formed between **5** and the self-complementary DNA duplex d(AATCTTTAAAGATT)$_2$. In contrast to the hydrogen-bonding interactions which predominate in the case of DNA adducts of sibiromycin, anthramycin, and tomaymycin, in the case of **5** we found that the high binding affinity appears to depend mainly on hydrophobic (van der Waals) interactions. Furthermore, high-resolution 2D NOESY data obtained with short mixing times allowed unequivocal determination of the orientation of the PBD molecule (A-ring toward 3′-end of covalently bound strand) and, in conjunction with DQF-COSY data, the stereochemistry at the C11 position (C11*S*). In addition, the 2D NOESY data allowed determination of the conformation of the C2-naphthyl ring, showing that it extends along the floor of the minor groove thereby optimizing hydrophobic interactions with DNA bases. These results provide opportunities for future drug design in terms of extending planar hydrophobic groups at the C2 position of PBDs to maximize binding affinity.

EXPERIMENTAL PROCEDURES

Oligonucleotide Synthesis and Purification. The 14-mer oligonucleotide 5′-AATCTTTAAAGATT was synthesized using an Applied Biosystems 391 DNA synthesizer employing a solid-phase β-cyanoethyl phosphoramidite synthetic protocol. The 5′-dimethoxytritylated oligonucleotide was removed from the synthesis column and treated with concentrated aqueous ammonia (10 mL) at 60 °C overnight. This was followed by purification using reversed-phase HPLC (BioCad Sprint, R3 column: 10 × 100 mm, flow 4 mL/min) at room temperature. Before starting the purification process, the column was equilibrated with 3 column volumes (CV) of buffer A (100 mM aqueous NH_4OAc, pH 10.0). Elution started with a washing gradient of 0−15% of 2 CV of buffer B (100 mM aqueous NH_4OAc/MeCN, 1:1 v/v, pH 10.0) which was held for 6 CV before returning to 100% buffer A. The total gradient run used 8 CV. Next, detritylation with TFA (2%) was performed (flow 0.5 mL/min), and the column back-washed with buffer A using 5 CV. Final gradient elution (using 8 CV, 0−40% buffer B) released the DNA from the column as monitored by optical density. Excess water was then removed under reduced pressure at 25 °C (Eppendorf Concentrator 5301), and the sample was subjected to dialysis against water using a cellulose membrane (Spectra/Por CE, 2000 MW cut-off, 5 mL volume) to afford ~10.0 mg of the pure oligonucleotide.

Formation of Annealed Duplex. The self-complementary

[2] National Cancer Institute (NCI) 60-cell-line panel gave GI_{50} mean values (MG-MID) of <1.0 nM for **5** and 33 nM for sibiromycin.

DNA strands were re-suspended in 0.5 mL of 90% H_2O/10% D_2O buffer solution (10 mM sodium phosphate/100 mM NaCl, pH 6.85) and heated at 65 °C for 5 min in a water bath. The solution was then slowly cooled to 25 °C and allowed to stand at this temperature for 16 h. This procedure was repeated to ensure proper annealing.

DNA Adduct Synthesis and Purification. The duplex DNA solution prepared above (0.5 mL) was incubated with **5** (7.5 mg as a slurry) at 37 °C for 48 h with gentle continuous shaking (Eppendorf Thermomixer Comfort). Excess **5** was then removed by filtration (Millipore 25 mm syringe filter, 0.45 μm pore size) and the filtrate collected directly in an NMR tube. This purification method was independently verified by repeating the procedure with **5** alone in D_2O followed by ^{1}H NMR analysis of the filtrate. This demonstrated that the concentration of **5** in the filtrate was below the limit of detection even after a high number of scans (1048). Presumably a sufficient concentration of **5** existed in solution to react with the DNA, thus causing more solid to dissolve to maintain a saturated solution, a process that continued until adduct formation was complete.

Thermal Denaturation Assays. (a) Calf Thymus DNA. **5** was subjected to DNA thermal melting (denaturation) studies using calf thymus DNA (CT-DNA, type I, highly polymerized sodium salt; 42% G + C (Sigma)) at a fixed 100 μM (in DNAp, equivalent to 50 μM in base pairs (bp)) concentration, quantitated using an extinction coefficient of 6600 (M phosphate)$^{-1}$ cm^{-1} at 260 nm. A solution of CT-DNA was prepared in pH 7.00 ± 0.01 aqueous buffer containing 10 mM NaH_2PO_4/Na_2HPO_4 and 1 mM Na_2EDTA (all AnalaR grade). A stock solution of **5** was prepared using DMSO. A working solution containing CT-DNA (50 μM in bp) and **5** (20 μM) was incubated at 37.0 ± 0.1 °C for 0−72 h using a Grant GD120 water bath.

Denaturation was monitored at 260 nm using a Cary 4000 UV−visible spectrophotometer fitted with a Peltier heating accessory. A precision probe calibrated to ±0.01 °C in the −10 to +120 °C range was used for temperature measurements. Heating was applied at a rate of 1 °C min^{-1} in the 50−98 °C temperature range, with optical and temperature data sampling at 0.10 °C intervals. A separate experiment was carried out using buffer alone, and this baseline was subtracted from the DNA melting curve before data treatment. Optical data were imported into the Origin 5 program (MicroCal Inc., Northampton, MA) for analysis. The DNA helix → coil transition temperature (T_m) was determined at the midpoint of the normalized melting profile. The result was obtained as the mean ± standard deviation from at least three determinations. Ligand-induced alterations in DNA melting behavior (ΔT_m) are given by $\Delta T_m = T_m$(DNA + ligand) − T_m(DNA), where the T_m value determined for native CT-DNA is 67.82 ± 0.07 °C (averaged from ∼110 previously accumulated runs). The working solution of **5** contained ≤0.3% v/v DMSO; the T_m result was corrected for the effects of DMSO co-solvent using a linear correction term determined for calibration mixtures.

(b) d(AATCTTTAAAGATT)$_2$. Thermal denaturation experiments on the **5**−d(AATCTTTAAAGATT)$_2$ adduct were conducted using a Cary 300 UV−visible spectrophotometer and 1 cm quartz cuvettes. Absorbances for the d(AATCTTTAAAGATT)$_2$ duplex alone (3.8 μM in duplex, equivalent to 53.2 μM in base pairs; extinction coefficient 2.14 × 10^5 M (duplex)$^{-1}$ cm^{-1} at 260 nm) and the **5**−d(AATCTTTAAAGATT)$_2$ adduct (4.4 μM concentration, equivalent to 61.6 μM in base pairs) were monitored at 260 nm as a function of temperature, as described above. The cuvettes were mounted in a thermal block, and the solution temperature was monitored using a thermistor in a reference cuvette. A computer-controlled heating rate of 0.5 °C min^{-1} from 15 to 95 °C was used, and the data were processed as described above for the experiments with CT-DNA.

NMR Experiments. All one- and two-dimensional NMR experiments were carried out using a Bruker Avance-500 spectrometer. The NMR spectra of the oligonucleotide duplex alone and the **5**−DNA adduct were recorded in the same buffer as used for the annealing process. The HOD peak was suppressed by using excitation sculpting with gradient pulse sequences (*26*). Chemical shifts are reported relative to 3-(trimethylsilyl)propionic acid-d_4 sodium salt.

2D NOESY spectra (pulse sequence taken from the Bruker Library: noesyesgpph) in the same solvent were acquired at 298 K with a spectral width of 10,000 Hz and 80 scans/increment using five different mixing times (50, 100, 150, 200, and 250 ms). 2D TOCSY spectra (pulse sequence taken from the Bruker Library: dipsi2esgpph) were recorded with a spectral width of 10,000 Hz and 60 ms mixing time. DQF COSY spectra (pulse sequence taken from the Bruker Library: cosydfesgpppph) were acquired at 298 K with a spectral width of 10,000 Hz and 48 scans with increased resolution of 16K in t_2 before zero filling to provide information for coupling constant measurements. All spectra were acquired in TPPI mode, and water suppression was achieved by excitation sculpting (*26*). 1D and 2D NMR data were processed using TopSpin 1.3 (Bruker Biospin), and assignments were assisted by Amix 3.0 (Bruker Biospin) using the Linux operating system. Phase-shifted skewed sine bell functions were used for apodization of the free induction decays, and Fourier transformed 2D spectra were manually phased and baseline corrected but not symmetrized.

Molecular Modeling of DNA and PBD−DNA Adducts. The starting structures for the DNA sequence were built using the ECCE software (*27*) loaded with the DNA toolkit sequence and saved in Brookhaven Protein Data Bank (PDB) file format. The structures of **5** and the naturally occurring PBDs were built with the ChemSketch-ACDLabs software (Advanced Chemistry Development, Toronto, Canada). These were imported into Maestro Version 6.5 (Schrödinger, Portland, OR) where MacroModel (*28*) (Schrödinger Ltd., Portland, OR) was used to perform the conformational search. Structures were minimized using AMBER force field parameters (*29*), and the effects of water as solvent were taken into account through the GB/SA implicit solvent model (*30*). The resulting structures were used as the starting point for a 200 step Monte Carlo (*31*) conformational analysis on each molecule. The energy window was set at 20 kJ mol^{-1} above the lowest energy conformation, and enantiomer distinction was required. Representative structures were selected based on a cluster membership through the cluster analysis program XCluster (*32*).

GRID calculations were performed to define the oligonucleotide surface for the docking process using the Greater graphical users interface (GRID Software Package, Molecular Discovery Ltd.). The docking process was performed with the Glue software package (GRID Software Package, Mo-

lecular Discovery Ltd.) establishing the DNA sequence as the target using a grid cage that included the three base pairs identified as the binding site (i.e., AGA) and **5** as the ligand. Docking was carried out taking into account electrostatic interactions and five rotatable bonds. The conformation and orientation of the molecules were verified using the Gview application (GRID Software Package, Molecular Discovery Ltd.). The structures that provided a better fit and lower energy of interaction were selected for further analyses. *Ab initio* calculations were carried out using Jaguar 6.0 software (Schrödinger Ltd., Portland, OR) and hybrid basis set B3LYP/6-31G**.

The previously designed DNA sequences were also imported into the Maestro 6.5 package. The ligand−DNA adducts were built by manually docking ligands (**1**, **2**, **3**, and **5**) and creating the covalent linkage between N2 of guanine and C11 of the PBD. MacroModel was used to locate the most stable conformation of adducts using 4000 steps of conformational search as described above.

NOE-Based Restrained Molecular Dynamics Simulations. Distance restraints were calculated from three-dimensional NOESY peak volumes based on the exponential function $d = r^{-6}$, as a function of mixing time (50 ms). The NOE intensities were collected using AMIX-Viewer 3.0 by selecting the NOESY contour plot recorded with 50 ms mixing time followed by normalization and integration. The additional set of NOE intensities from 250 ms mixing time was collected by overlapping the 50 and 250 ms 2D NOESY contour plots and picking peaks present in the 250 ms NOESY spectrum but absent from the 50 ms spectrum. The direct spin−spin system (H5−C4 × H6−C4) provided the reference volume for integrating the remaining cross-peaks (2.45 Å fixed distance). The initial set of X-PLOR coordinates was refined using the NOE-based distance restraints as an input file in two steps: (i) distance restraints from the NOESY experiment at 50 ms mixing time; (ii) additional distance restraints from the NOESY experiment at 250 ms mixing time. These X-PLOR distance restraint files were used in restrained molecular dynamics simulation (RMDS) in order to investigate incompatible assignments through distance violations proposed by the molecular graphics software (VMD-XPLOR 2.1.6). Distance restraints for nonexchangeable protons in the NOESY experiment at 50 ms mixing time were constrained within $d \pm 20\%$ as a penalty function (square deviation). All distance constraints from the 50 ms NOESY spectrum were distributed according to cross-peak intensities as strong (S) 1.80−2.90 Å or medium (M) 1.80−4.00 Å. Distance constraints with methyl protons were considered as alternative functions for the three protons with fixed restraints ($d = 4.0$ Å, −1.0/+1.5 Å). Fixed range distance restraints ($d = 4.0$ Å, −2.2/+1.0 Å) were enforced to all cross-peaks from the 250 ms mixing time NOESY experiment, except for methyl protons ($d = 4.0$ Å, −2.2/+1.5 Å). All RMDSs were carried out with X-PLOR NIH 2.18 using the simulated annealing approach. Initial RMDSs were performed *in vacuo* at 1,000 K (2,000 steps) without considering solvent or counterion effects. Final relaxation refinement involved RMDS with explicit solvent at 2,000 K, and the system was then allowed to cool down in over 2,000,000 steps (0.1 ms) to 300 K (bath temperature). This was repeated 200 times with the experimental restraints. The 10 lowest energy structures (out of 200) were analyzed using VMD-XPLOR (*33*) and the root-mean-square deviation values are reported in Table 2.

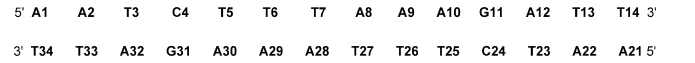

FIGURE 2: Schematic representation of d(AATCTTTAAAGATT)$_2$ showing the numbering system used for identifying each nucleotide. Numbering of both strands was necessary to distinguish cross-peaks assigned to protons on opposite strands (interstrand cross-peaks).

RESULTS AND DISCUSSION

Choice of Oligonucleotide Sequence for NMR Study. The selection of the DNA sequence for the NMR study was based on previous knowledge of PBD binding preference and the *in silico* docking of **5** into a designed duplex. In particular, the oligonucleotide had to contain a purine−G−purine triplet for the PBD to covalently bind to (*16*). Also, in order to allow the PBD to bind in either the 3′- or 5′-orientation, and to test the hypothesis that the agent would prefer to bind with its A-ring oriented 3′, the oligonucleotide had to be long enough to accommodate the molecule in both directions. Additionally, the oligonucleotide was required to be self-complementary to simplify NMR interpretation but without introducing additional guanine residues as potential alternative PBD binding sites. Two sequences were initially proposed, sequence A with 12 bp that included a 2 bp spacer between the two PBD (5′-AGA ≡ 3′-TCT) binding sites and sequence B in which this spacer is extended to 4 bp (binding sites are highlighted in bold): Sequence A, 5′-AA**TCT**TA**AGA**TT-3′; Sequence B, 5′-AA**TCT**TTAA**AGA**TT-3′. Sequences A and B were subjected to preliminary GRID (*34*) calculations, and docking analyses were carried out using the Glue package with a flexible ligand (**5** in its imine form). The results showed a negative energy of interaction between **5** and both sequences (Supporting Information) indicating favorable binding in either case. However, the greater distance between the two drug molecules in sequence B minimized any potential overlap.

Proton Assignments for DNA Sequence d(AATCTTTAAAGATT)$_2$. Initially, a set of ^{1}H 1D and 2D NMR spectra of the annealed oligonucleotide was obtained and progressively assigned starting from the exchangeable protons. The nucleotide numbering sequence used for the assignments is shown in Figure 2. The observation of imino signals and imino−imino sequential connectivities at 12.3−14.2 ppm in the ^{1}H NMR and 2D NOESY spectra indicated DNA duplex formation. Cross-peaks between the imino and H2 of adenines (intranucleotide) and between imino and H1′ were also analyzed in the 2D NOESY spectrum, as these protons are critical for interaction with the PBD molecule. Nonexchangeable hydrogen signals were progressively assigned starting from the sequence-specific NOEs between the base (H6 and H8, 7.1−8.2 ppm region) and the deoxyribose (H1′, 5.4−6.3 ppm) protons at 200 ms mixing time. All other protons, except the glycosydic H5′/H5′, were assigned, and the NOE-derived distance constraints were found to be consistent with a B-type DNA spectrum (see Supporting Information for assignments).

Synthesis and NMR Assignment of the Water-Soluble C11-Bisulfite Form of **5.** All previously reported NMR studies of PBD−DNA adducts have suffered from the problem that PBD molecules, in general, are not highly water soluble, and

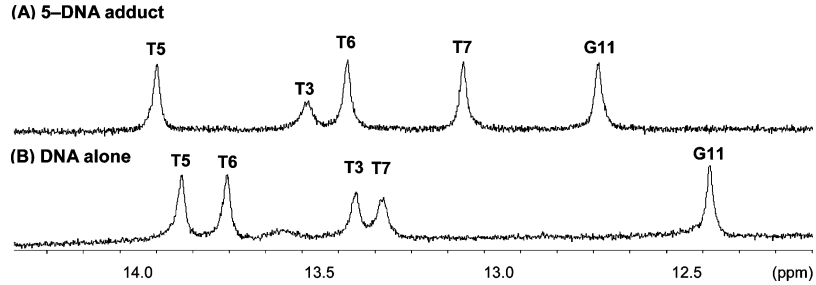

FIGURE 3: Expanded 1D ^{1}H NMR spectra of the imino region for the **5**−DNA adduct (A) and the DNA alone (B). Clear chemical shift differences were observed for the NH-imino protons of the covalently modified G11 base. Differences were also observed for the neighboring T3, T5, T6, and T7 bases.

so initial assignments of the PBD molecule alone in D_2O could not be obtained. To address this problem, we synthesized **6** (Figure 1), a highly water-soluble C11-bisulfite form of **5**. PBD C11-bisulfite adducts have previously been reported to retain the biological activity of parent PBDs while having improved water solubility (*35, 36*). **6** was synthesized from **5** in 67% yield as an epimeric mixture using a simple one-step process (sodium bisulfite in DCM) (*37*). Unlike the free imine form **5**, it was readily soluble in D_2O, and all proton signals could be assigned (see Supporting Information).

Adduct Formation. Due to the limited water solubility of **5**, the DNA adduct could be prepared by simply mixing the annealed duplex DNA with an excess of **5** in D_2O-containing buffer followed by gentle shaking for 48 h at 37 °C. During this time the small amount of **5** in solution was able to react covalently with the DNA until reaction was complete. The solid excess of **5** ensured that the solution was always saturated and could be simply filtered off when reaction was complete. This left pure adduct in solution together with a small quantity of **5** too dilute to be detectable in the NMR spectrum.

Formation of an adduct between **5** and DNA was initially confirmed by melting studies (T_m = 36 °C for duplex alone; 64 °C for the **5**−DNA complex). This ΔT_m shift (28 °C) was significantly higher than expected (e.g., ΔT_m for **5** with native CT-DNA is 15.8 °C) but may reflect an accumulative effect of binding two PBD molecules within a relatively short sequence of DNA with high affinity. Furthermore, the probability of occurrence of Pu-G-Pu sites in the calf thymus DNA used in this analysis (<10.5%) is lower than in d(AA**TCT**TTAA**AGA**TT)$_2$ (16.7%). Alternatively, there may be a binding-induced cooperative effect for the two close sites in d(AA**TCT**TTAA**AGA**TT)$_2$, such that accommodation of the first PBD ligand results in enhanced binding affinity for the second ligand (*38*).

NMR Assignments for the **5**−*DNA Adduct. (a) Exchangeable Proton Assignments.* The imino−imino sequential NOE connectivities for the sequence fragment 5′-TCTTT-3′•5′-AGAAA-3′ revealed that the Watson−Crick stacking/alignment had been preserved from the original DNA sequence (see Supporting Information). However, the imino region of the **5**−DNA complex differed substantially from that of the DNA alone (Figure 3). As anticipated, the guanine NH imino (G11) had shifted significantly from 12.30 to 12.80 ppm, due to formation of the new covalent bonds in close proximity. In addition, the 12.80 ppm G11 signal exhibited NOEs with the 8.31 ppm signal of the N10 PBD proton and the 6.42 ppm signal due to the exposed amino protons of C24 on the opposite strand. These NOE cross-peaks indicate that the G11-C24 base pair has not been totally disrupted, which is further supported by the cross-peaks observed between the imino (12.0 to 14.0 ppm) and aromatic H2 (6.5 to 8.1 ppm) protons.

(b) Nonexchangeable Proton Assignments. The nonexchangeable protons of the **5**−DNA adduct were assigned starting from identification of the cross-peak between H5 and H6 of the cytosine in the TOCSY experiment. The pattern of sequential NOE connectivities observed between the deoxyribose H1′ and base H8/H6 protons (Figure 4) suggested that the B-form structure observed in the duplex alone had been retained in the adduct. The presence of C2′-endo sugar geometry was confirmed by the NOEs between the glycosidic H2′/H2″ and aromatic H8/H6 protons (see Supporting Information). Additionally, a comparison between the chemical shifts derived from the two sequential assignments (i.e., DNA alone and the adduct; Figure 5) revealed that the chemical environment of the **5**−DNA adduct had not been substantially affected in the aromatic region. However, the H1′ protons of cytosine 24 and thymines 25 and 26 on the opposite strand at the lesion site were significantly affected. Specifically, H1′ of the covalently modified G11 shifted downfield from 5.49 to 5.83 ppm. The reason for this different behavior is that the H6/H8 protons are located in the major groove, whereas the H1′ protons are in the minor groove. Therefore, H1′ is more likely to be affected by the insertion of **5**. Not surprisingly, the chemical shifts (δ) of these glycosidic H1′ protons exhibit the highest positive and negative $\Delta\delta$ values, as represented by the blue line in Figure 5.

Assignment of signals for **5** within the adduct spectrum was assisted by the data obtained for the water-soluble bisulfite analogue **6** in D_2O. The H9 (6.58 ppm), H6 (7.16 ppm), and H3 (8.05 ppm) protons could be readily identified from the 2D NOESY spectrum, and assignment of the naphthyl protons was achieved by overlapping the TOCSY/NOESY contour plots (see Supporting Information). Similarly, the H11, H11a, H1α, and H1β protons were assigned by overlapping the COSY/NOESY counter plots which clearly exposed the through-bond interactions between the H11 and H11a protons of **5** (5.84 × 4.13 ppm).

In Silico Structural Analysis of **5** *and the* **5**−*DNA Adduct.* The docking of **5** (in the imine form) into the 5′-A**AGA**T-3′ binding site of the duplex DNA was modeled using GRID (GRID Software Package, Molecular Discovery Ltd.) (*34*) (see Supporting Information). The most favorable conforma-

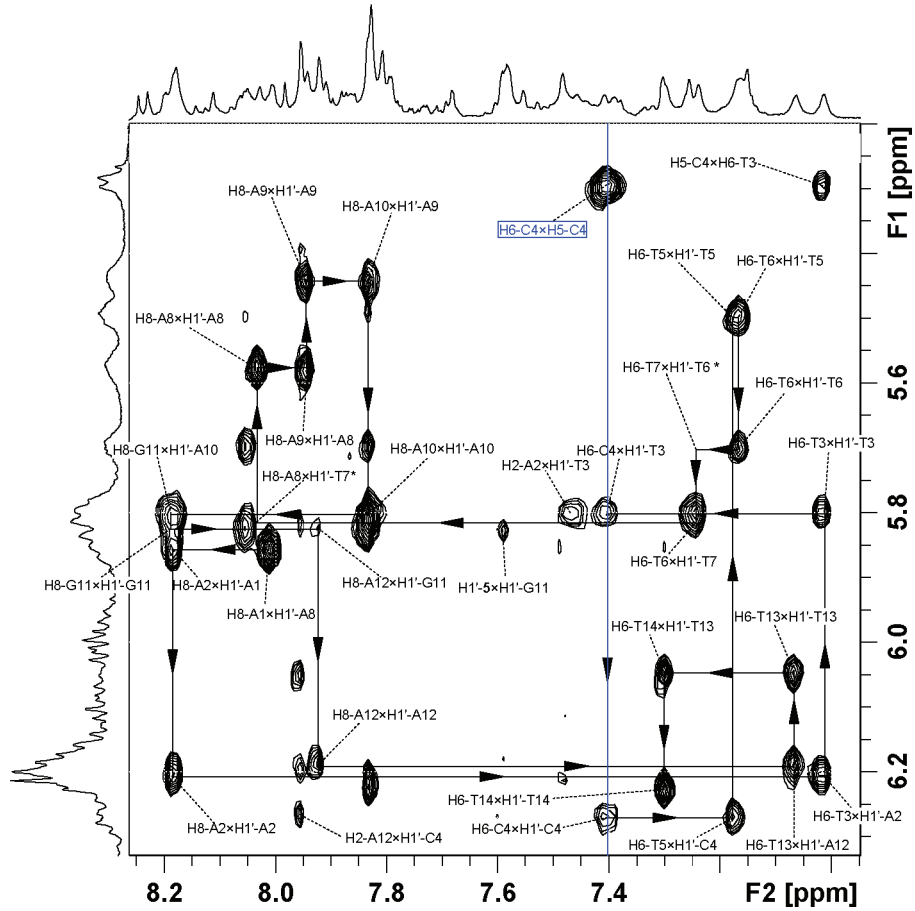

FIGURE 4: Expanded contour plots of the **5**−DNA adduct NOESY experiment in D_2O at 298 K and 500 MHz (250 ms mixing time) showing intrastrand sequential connectivities between the nonexchangeable base (H6 and H9) and deoxyribose (H1′) protons. The H6−C4 × H5−C4 cytosine cross-peak is highlighted in blue. This cross-peak was also observed in the TOCSY experiment and provided the starting point for the sequential assignment. (*, visible only at lower cutoff).

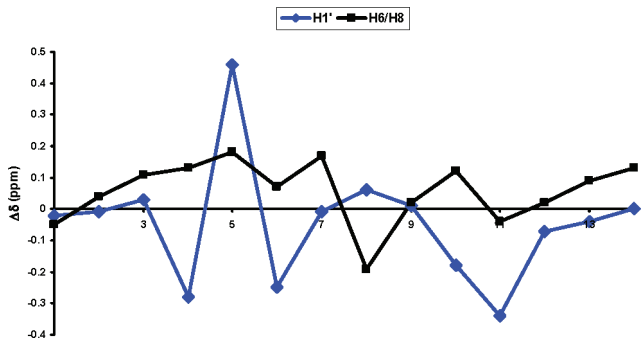

FIGURE 5: Differences in the chemical shifts of the glycosidic H1′ and aromatic H6 or H8 protons for the DNA sequence alone versus the **5**−DNA adduct.

tion of the docked **5** molecule indicated that its A-ring prefers to orient toward the 3′-end of the covalently modified DNA strand.

For comparison purposes, the DNA adducts of three naturally occurring PBDs (sibiromycin, anthramycin, and tomaymycin) and **5** were subjected to a conformational search using the same DNA sequence and binding site (5′-AA**AGA**TT-3′). Figure 6 compares the lowest energy adducts of **5**, sibiromycin, anthramycin, and tomaymycin, all with C11(*S*) configuration of the PBD and with their A-rings oriented toward the 3′-end. This analysis indicated a varying degree of hydrogen bonding between the PBD molecules and the adjacent DNA bases (see Table 1). Sibiromycin and anthramycin both have hydroxyl groups at their C9 positions which can form H-bonds with the opposite-strand cytosine O2 of the C24/G11 base pair. It was also found that the C7-sugar moiety of sibiromycin can adopt two possible conformations (only one is shown in Figure 6), both of which can provide H-bonds to the phosphate backbone of the opposite strand, thus further stabilizing the adduct. Although the X-ray structure of the anthramycin adduct revealed that the amino group of the C2-acrylamide tail forms a H-bond to the carbonyl group of the cytosine residue on the same strand, this was not evident from our own analysis where an adenine replaced the cytosine residue and the acrylamide tail was not sufficiently close to form a H-bond. Therefore, taken together with the H-bond donated by the N10-H of all these PBDs, a sum of three and two potential H-bonds for this particular DNA sequence was found for sibiromycin and anthramycin, respectively, with either two (sibiromycin) or one (anthramycin) formed to the opposite noncovalently bound strand. In contrast, tomaymycin has only the C8-hydroxyl (in addition to the N10-H) as a potential hydrogen bond donor, although the position of this substituent pointing along the DNA minor groove does not allow it to form any hydrogen bonds to DNA bases. Similarly, **5** has only the N10-H group available for H-bonding with the adjacent thymine on the covalently modified strand and so should have a similar DNA-interactivity profile to tomaymycin.

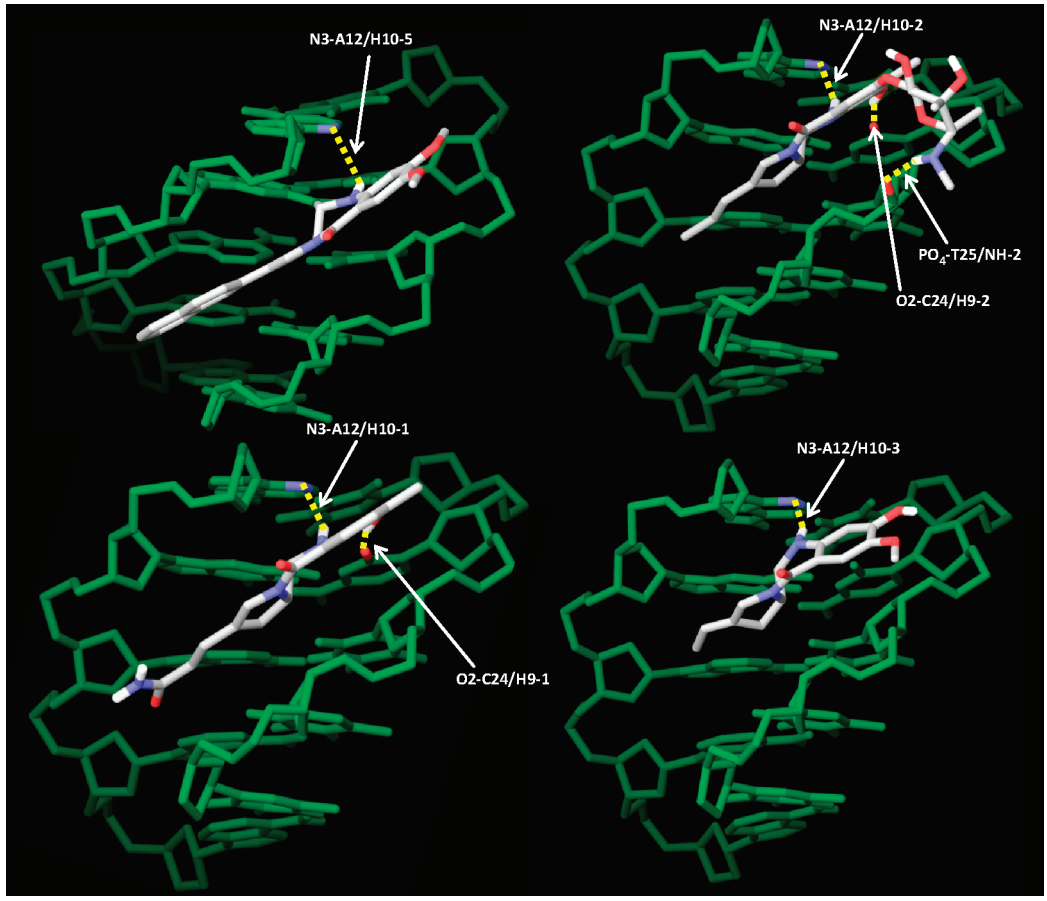

FIGURE 6: Energy-minimized models (based on Monte Carlo conformational searches) of PBD−DNA adducts of **5** (top left), sibiromycin (top right), anthramycin (bottom left), and tomaymycin (bottom right) covalently attached to the central guanine of d(5′-TAAGATT-3′)$_2$. In each case the PBD is oriented with its A-ring toward the 3′-end of the covalently modified strand and with *S*-stereochemistry at the C11 position. DNA is depicted in green (with blue N and red O atoms if involved in H-bonds, and the PBDs are colored using the CPK scheme. Feasible H-bonds between **5** and DNA (i.e., <4.0 Å) are shown as dashed yellow lines. Nonpolar H atoms are omitted for clarity.

Table 1: ΔT_m Values for Thermal Stabilization of Native Double-Stranded Calf Thymus (CT) DNA by **1**−**3** and **5** and Number of Feasible H-Bonds Generated between Each of These Ligands and DNA Bases When Bound Covalently in an Energy-Minimized Adduct to the Guanines of d(AA**TCT**TTAA**AGA**TT)$_2$

		No. of H-bonds between PBD and DNA		
compound	ΔT_m[a] (°C)	modified strand[b]	opposite strand	total
1 (anthramycin)	13.0	1	1	2
2 (sibiromycin)	16.3	1	2	3
3 (tomaymycin)	2.6	1	0	1
5 (C2-naphthyl PBD)	15.8	1	0	1

[a] ΔT_m values for **1**, **2**, and **3** are taken from ref *40*. [b] DNA strand covalently modified by the ligand.

Table 1 also provides the calf thymus ΔT_m values for these PBDs, and for **1**−**3** there appears to be a relationship between their ability to stabilize DNA and the number of hydrogen bonds that can form within the adducts. The interesting feature of this analysis is that PBD **5** can only form one hydrogen bond per Pu-G-Pu site on calf thymus DNA but causes a dramatic shift in melting temperature of 15.8 °C. The most likely explanation is that the molecule makes a number of favorable hydrophobic contacts with DNA bases thereby stabilizing the adduct.

Orientation, C11 Configuration, and C2-Naphthyl Conformation from NOE-Based NMR Data. (a) C2-Naphthyl PBD Orientation. According to the accepted mechanism of action of naturally occurring PBDs, the H1α, H1*β*, H11a, N10-H, and H9 protons should be the most likely to provide NOEs with host DNA protons due to their close proximity (i.e., facing the floor of the minor groove). This was confirmed through the NOESY experiment using a 50 ms mixing time, with strong NOEs observed between the H9 proton of **5** and surrounding DNA protons toward the 3′-end of the covalently modified strand. For example, strong NOEs were detected between H9-**5** (6.60 ppm) and H2 (7.96 ppm) of A12 and H1′ (6.27 ppm) of C24 on the opposite strand. Similarly, a NOE cross-peak (3.98 × 7.96 ppm) could be assigned for the protons of 8-OCH$_3$-**5** and H2-A12. A weak NOE was also observed between H9-**5** (6.50 ppm) and H1′ (6.06 ppm) of T23. In the case of the NOESY experiment with a 250 ms mixing time, a NOE between H9-**5** (6.60 ppm) and the imino proton H1 (12.80 ppm) of G11 was detected along with the cross-peak (3.98 × 2.41 ppm) corresponding to 8-OCH$_3$-**5** and H2″-T23 on the opposite strand. These unambiguous assignments obtained from experiments at two different mixing times have allowed the unequivocal determination of the orientation of **5** in the DNA minor groove, thus complementing previously published NMR (*9, 10*) and crystallographic structures (*12*) of anthramycin−DNA adducts.

(b) C11 Stereochemistry of Bound C2-Naphthyl PBD. Since the NMR data clearly indicated the orientation of the PBD molecule, there were four possible arrangements for the

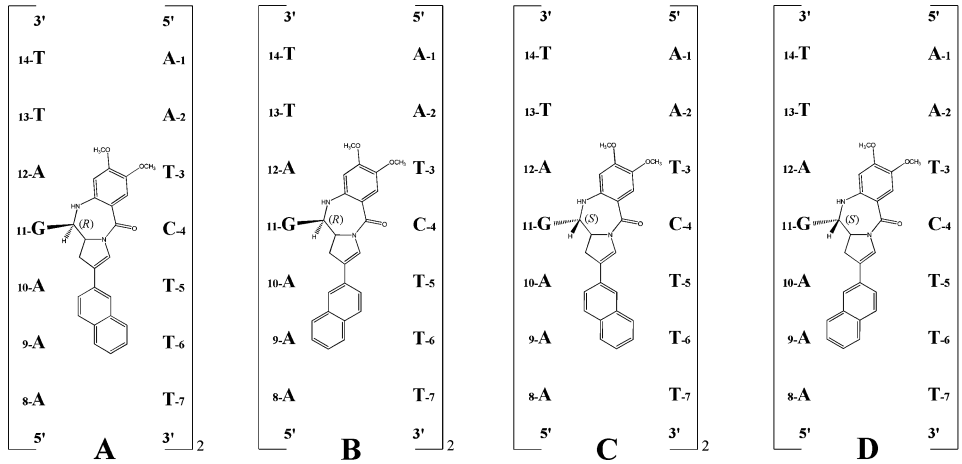

FIGURE 7: Four possible arrangements of the **5**−DNA adduct with different stereochemistry at C11 (A, B = *R*; C, D = *S*) and two different orientations of the C2-naphthyl group. In each model the PBD is oriented with its A-ring toward the 3′-end of the covalently modified strand.

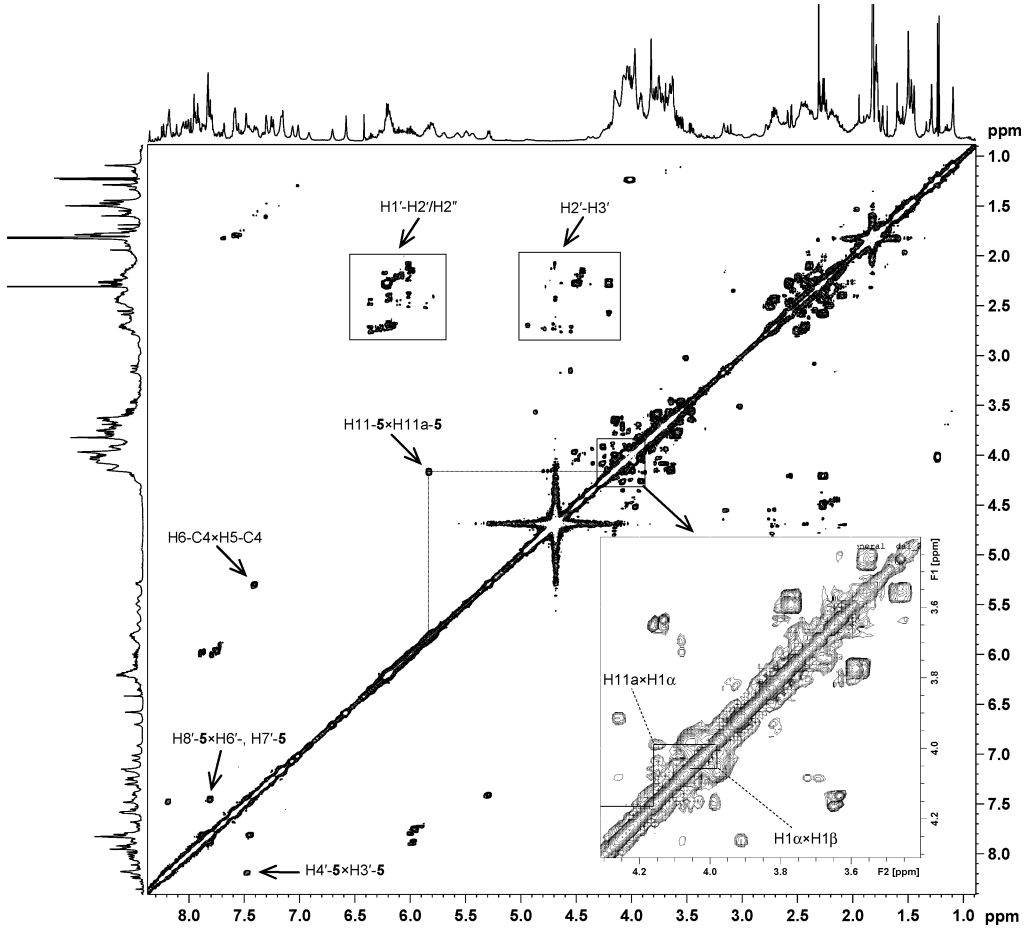

FIGURE 8: COSY experiment on the **5**−DNA adduct in D_2O showing the PBD and DNA nonexchangeable proton through-bond connectivities. In support of a C11*S* configuration for the covalent linkage between the PBD and DNA, the relevant H11-**5** × H11a-**5** cross-peak (5.84 × 4.13 ppm) is highlighted along with expansions of the H11a-**5** × H1α-**5** and H1α-**5** × H1*β*-**5** through-bond connectivities (inset).

adduct (Figure 7) relating to the choice of *R* or *S* stereochemistry at the C11 position of the PBD and two different conformations of the C2-naphthyl substituent. The C11 stereochemistry could not be immediately assigned using the reference H11a-**5** signal because the H11a-**5** × H11-**5** NOESY cross-peak overlapped with the glycosidic H1′ × H4′ NOE region. Nevertheless, a C11(*S*) configuration could be initially assigned based on the NOESY contour plot analysis of the H11-**5** and DNA protons exposed in the minor groove. A cross-peak between H1′-A12 and H11-**5** (6.19 × 5.84 ppm) was observed in the NOESY spectrum at 50 ms mixing time. Furthermore, a NOE was observed between H11-**5** and the imino protons NH-G11 (5.84 × 12.80 ppm) at 250 ms mixing time. This spatial arrangement is only satisfied if the H11-**5** proton points toward the adjacent A12 nucleotide (i.e., with H11 in an "*anti*" orientation relative to H11a). In addition, a high-intensity cross-peak (i.e., at the same cutoff level as the reference H6−C4 × H5−C4 through-bond spin system) was observed in the COSY spectrum (Figure 8) between the H11-**5** and H11a-**5** protons,

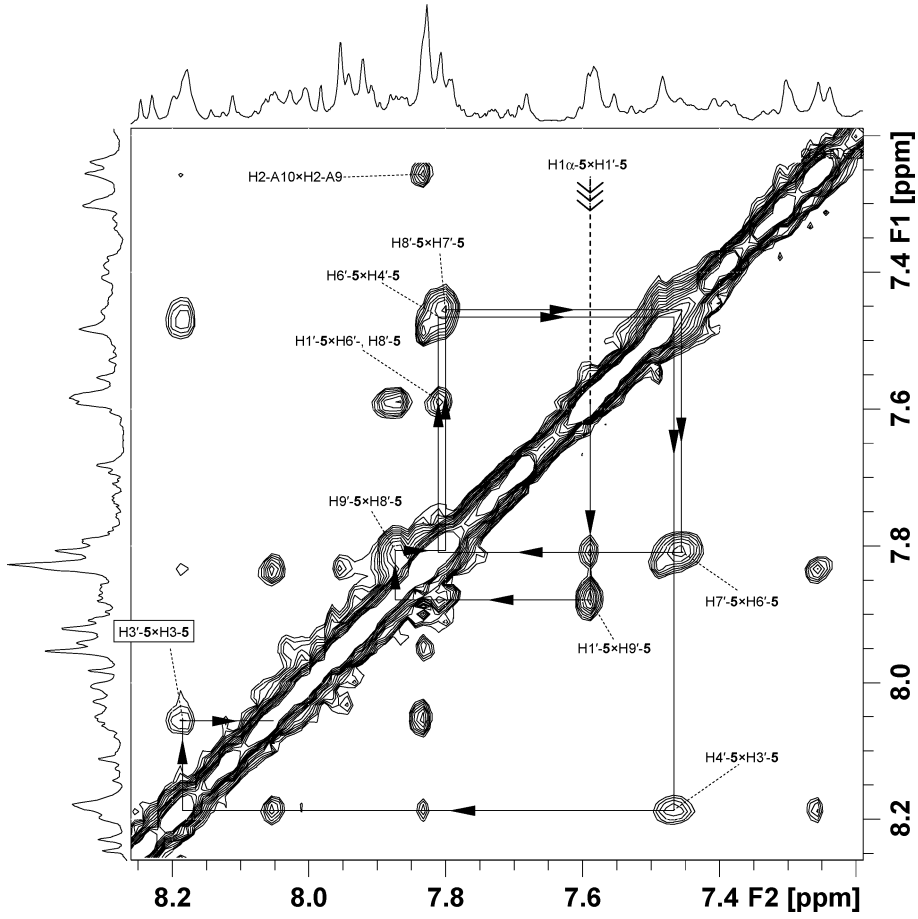

FIGURE 9: Expanded contour plot of the NOESY spectrum of the **5**−DNA adduct in D_2O at 298 K and 500 MHz (250 ms mixing time) showing intradrug sequential connectivities between the C2-naphthyl (H1′ to H9′) protons. All vicinal cross-peaks were also observed in the COSY and TOCSY experiments. The cross-peak defining the conformation of the C2-naphthyl ring is highlighted in blue.

suggesting a through-bond coupling with a *J* value >10 Hz, only possible with a C11(*S*) configuration (i.e., dihedral angles for the C11(*S*) and C11(*R*) configurations of 159° and 27°, respectively). A DQF-COSY experiment was used to determine the coupling constant of the H11-**5** × H11a-**5** cross-peak initially observed in the basic COSY spectrum. The *J* value of 10.6 Hz found for this cross-peak confirmed that H11 must be in an "*anti*" direction relative to a *S*-configured H11a proton.

(c) Conformation of the C2-Naphthyl Fragment. The conformation of the C2-(2-naphthyl) substituent, which could reside in one of two possible orientations, was investigated via the NOE cross-peaks between **5** and the DNA protons in the minor groove. The naphthyl protons were initially traced out by overlapping the contour plots of the TOCSY and NOESY spectra (see Supporting Information). The resonance signals of the set of seven protons belonging to the naphthyl fragment overlap in the two subsets; i.e., H4′-**5** and H7′-**5** (7.45−7.47 ppm) and H6′-**5** and H8′-**5** (7.79−7.80 ppm), with H9′-**5** shifted slightly to 7.85 ppm and the two remaining peaks assigned as H1′-**5** (7.60 ppm) and H3′-**5** (8.2 ppm). The naphthyl protons are interconnected, which allowed them to be sequentially assigned through NOE connectivities (Figure 9). Two strong intraligand NOEs were observed at 50 ms mixing time between the H3′-**5** and H3-**5** (8.20 × 8.05 ppm) and H1α-**5** and H1′-**5** (3.98 × 7.60 ppm) protons, which were important for elucidating the preferred conformation. Another NOE cross-peak at 4.13 × 7.60 ppm was assigned to H11a-**5** × H1′-**5** which, in conjunction with the previous NOEs, suggested that the H3′-, H4′-, and H6′-**5** protons were situated on the outer face of the minor groove with the H1′-**5** and H9′-**5** protons lying along the lipophilic floor. Further evidence for this "inward" conformation was provided by two additional NOEs recorded at 250 ms mixing time between **5** and DNA protons exposed in the minor groove. A strong NOE was detected between H1′-**5** and H2-A10. Similarly, H7′-**5** and H4′-T27 (opposite strand) exhibited a strong cross-peak (7.45 × 4.07 ppm) in the NOESY spectrum. In addition, a weak NOE was observed between H9′-**5** and the same T27 sugar protons (7.85 × 4.07 ppm), thus indicating a conformation for the "D ring" in which the H9′-, H8′-, and H1′-**5** protons are positioned close to the floor of the minor groove (Figure 7, adduct D).

Restrained Molecular Dynamics and NOE-Based Refinement. The calibrated NOE cross-peak intensities, derived from 50 and 250 ms two-dimensional NOESY spectra measured in 10% D_2O/90% H_2O, were converted into distance restraints in X-PLOR (version NIH 2.18) using the cytosine H5−H6 cross-peak as an internal reference. The NOE-based constraints were employed for molecular dynamics simulations in separate sets to investigate incompatible assignments by observing distance violations using molecular graphic software (VMD version 1.86 as a part of VMD-XPLOR) (*39*). The starting structure (with C11(*S*) configuration of the PBD and with the A-ring oriented toward the 3′-end of the covalently modified strand) was initially proposed based on *in silico*, NOESY, and DQF-COSY experiments. Although the common RMD protocol considers

FIGURE 10: Overlap of the 10 lowest energy structures of the **5**−DNA adduct obtained by restrained molecular dynamics simulation (simulated annealing) using NOE-derived distance restraints.

the Watson−Crick set of H-bonds between purine and pyrimidine bases, the H-bonds of the AGA·TCT sections of the duplex were deliberately removed to allow free flexibility of the PBD and base pairs at the binding site. A total of 264 constraints were found in the NOESY spectrum recorded at 50 ms mixing time, of which 20 were derived from NOEs between **5** and the DNA matrix. Similarly, a set of 110 additional NOE cross-peaks were observed at 250 ms mixing time, with an additional 20 constraints derived from cross-peaks between **5** and the DNA, further demonstrating the close proximity of the ligand to the walls of the minor groove. Overlapping of the family of 10 lowest energy structures for the **5**−DNA adduct is shown in Figure 10. These structures are consistent with the Dickerson−Drew form of a B-DNA duplex, and Table 2 shows the structural refinement statistics.

Table 2: Statistics for the NOE-Based Set of Structures for the Symmetrical **5**−DNA Adduct (20 structures of which the 10 of lowest energy were accepted as a family)

Experimental Distance Constraints	
Observed at 50 ms Mixing Time	
intraresidue (S) 50; (M) 78; (CH_3) 16	144
intrastrand (S) 8; (M) 52; (CH_3) 20	80
interstrand	0
DNA−PBD (S) 2; (M) 18; (CH_3) 0	20
PBD−PBD (S) 14; (M) 6; (CH_3) 0	20
total	264
Observed at 250 ms Mixing Time (Additional)	
intraresidue	30
intrastrand	22
interstrand	18
DNA−PBD	20
PBD−PBD	20
total	110
Empirical Distance Constraints	
hydrogen bonds[a]	32
ligand dihedral angles	84
Structural Statistics	
distance violation per structure (>0.5 Å)	0
dihedral angle per structure (>5°)	0
Structure Quality	
rmsd (average for all atoms in the 20 lowest energy structures) (Å)	1.44
range for all atoms (Å)	0.65−2.28
rmsd (average for all atoms in the 10 lowest energy structures) (Å)	1.14
range for all atoms (Å)	0.59−1.54

[a] The H-bonds between the AGA·TCT section of the duplex were not included.

Effect of Covalent Bonding on the **5**−*DNA Structure and Interactions between* **5** *and the DNA Duplex.* The NOE-derived final structure shown in Figure 10 enabled the assessment of stabilizing forces beyond the covalent bond. The adduct consists of two PBD molecules in the minor groove covalently bound to each DNA strand with no spatial restrictions for binding of the two ligands. For each PBD molecule the C2-(2-naphthyl) substituent is orientated as if pointing toward the middle of the helix such that it lies along the minor groove with 5.8 degrees of flexibility within the C3−C2−C1′−C2′ dihedral angle. The final structure of the adduct revealed that **5** causes no major distortions within the DNA duplex and that the B-form observed prior to attachment of **5** is preserved. The most noticeable perturbation occurs at the two covalent binding sites where the presence of **5** appears to pull the two strands together compared to the rest of the duplex. As a consequence, the terminal 3′-CTAA-5′·3′-TTAG-5′ base-pairs buckle and incline slightly, but the Dickerson−Drew B-DNA structure is preserved overall. The lowest energy NOE-derived structure of the **5**−DNA adduct clearly shows that the DNA minor groove narrows significantly at the covalent attachment sites. This was confirmed by measuring the shortest phosphate−phosphate (P−P) distances between opposite strands of DNA (Table 3). These results demonstrate that the minor groove width narrows throughout the duplex but was found to be on average 2.5 Å shorter at the PBD binding sites compared to the same sequence without drug attached. The same

Table 3: Minor and Major Groove Widths for the **5**−DNA Adduct: Direct Phosphate−Phosphate (P−P) Distances (Å) and Refined P−P Distances[a]

	P−P	Refined	P−P	Refined
ideal[b]	11.7	11.7	17.0	16.9
$A^1A^2/T^{33}T^{34}$				
$A^2T^3/A^{32}T^{33}$				
$T^3C^4/G^{31}A^{32}$	10.1		18.5	
$C^4T^5/A^{30}G^{31}$	9.2	9.2	16.0	15.8
$T^5T^6/A^{29}A^{30}$	8.5	8.4	15.5	15.1
$T^6T^7/A^{28}A^{29}$	9.9	8.9	18.1	17.6
$T^7A^8/T^{27}A^{28}$	12.3	10.6	15.0	13.6
$A^8A^9/T^{26}T^{27}$	11.8	10.9	17.8	16.4
$A^9A^{10}/T^{25}T^{26}$	9.2	9.0	17.7	17.4
$A^{10}G^{11}/C^{24}T^{25}$	9.3	9.3	16.5	16.2
$G^{11}A^{12}/T^{23}C^{24}$	10.2		17.1	
$A^{12}T^{13}/A^{22}T^{23}$				
$T^{13}T^{14}/A^{21}A^{22}$				

[a] The distances were measured according to methodology described by El Hassan and Calladine (*41*). [b] Distances observed for an ideal geometry of B-form DNA alone.

methodology revealed that the major groove width had not significantly changed, providing further evidence that the B-form structure initially observed for the DNA duplex alone had been maintained upon interaction with **5**.

In addition, we found that the N10-H of **5** can form a hydrogen bond with N3 of the adjacent adenine 12 (2.08 Å) or, to a lesser extent, with O2 of cytosine 24 (3.43 Å). Previous X-ray studies (*12*) with anthramycin and a different DNA sequence found comparable interactions. However, the structure of anthramycin is substantially different from **5**; the additional 9-OH and C2-acrylamide functionalities allow anthramycin two additional hydrogen-bonding interactions with the base pairs adjacent to the G alkylation site which may account for its relatively high CT-DNA ΔT_m (13.0 °C). Interestingly, despite the higher ΔT_m (15.8 °C) of **5**, apart from the N10-H to N3-A12 hydrogen bond to the covalently modified strand that all PBDs form, it cannot form any further hydrogen bonds. Thus, insufficient hydrogen-bonding interactions are formed to explain the significant duplex stabilization caused by **5** compared to other molecules in the series (i.e., sibiromycin, anthramycin, and tomaymycin). Therefore, the helix stabilization is most likely explained by hydrophobic interactions between **5** and DNA.

It is known that the hydrophobic surfaces of DNA are confined to the floor of the minor groove, in close proximity to the N10-C11 moiety and the C2-naphthyl group of **5** which align with the curvature of the groove. This spatial relationship between the DNA and **5** is supported by the results in Figure 5 which show that the chemical shifts of the minor groove H1′ protons of G11 and T5 significantly change at the binding site. These changes may be attributed to the PBD molecule disturbing the sugar pucker around the alkylation sites. In fact, the final **5**−DNA adduct model (Figure 10) indicates that the H1′-T5 proton is separated by only 1.75 Å from H11a-**5**. Similarly, the nonexchangeable H1′-G11 and H11a-**5** protons are separated by 2.15 Å and the H1′-C24 and H9-**5** protons by 2.51 Å. As a consequence, it may be concluded that **5** lies closer to the floor of the minor groove to avoid the outer predominantly hydrophilic surfaces. This could contribute to overall duplex stabilization and may explain the high ΔT_m values for **5**.

CONCLUSIONS

The NMR structure of a symmetrical 2:1 adduct of the synthetic C2-(2-naphthyl) PBD **5** bound to a cognate DNA duplex has been determined and a molecular model produced. This structure provides an explanation for the unusually high DNA helix-stabilizing properties of **5** in that the molecule lies close to the floor of the minor groove and is stabilized predominantly by hydrophobic interactions. This behavior is in contrast to related PBD natural products such as sibiromycin and anthramycin which form two or more hydrogen bonds with DNA bases. In addition, the resolution of the structure obtained has been sufficient to determine the orientation of the PBD molecule (i.e., A-ring toward the 3′-end), the stereochemistry at the C11 position (i.e., *S*), and the conformation of the C2-naphthyl ring (i.e., close to the groove floor with "inward" orientation).

These findings could be important for the design of future generations of PBD-based compounds with higher DNA-binding affinity and enhanced sequence selectivity. The C2-naphthyl ring system is amenable to several synthetic modifications that could introduce hydrogen bond accepting/donating opportunities while maintaining the hydrophobicity required for highly efficient DNA binding. We are currently investigating new analogues of **5** with heteroatoms in the C2-naphthyl fragment to explore this possibility, and these results will the reported in due course.

ACKNOWLEDGMENT

Emma Sharp is thanked for her expert assistance in preparation of this manuscript. The Engineering and Physical Sciences Research Council is thanked for providing funding for the NMR instrumentation.

SUPPORTING INFORMATION AVAILABLE

^{1}H NMR, 2D NOESY, and full assignment of the $d(AATCTTTAAAGATT)_2$ duplex; synthetic methodology and NMR assignments for **6**; details of the **5**−DNA adduct proton assignments (including DQF-COSY data); tabulated chemical shifts of **5** in the **5**−DNA adduct; and *in silico* studies on the **5**−DNA adduct. This material is available free of charge via the Internet at http://pubs.acs.org.

REFERENCES

1. Thurston, D. E. (1993) Advances in the Study of Pyrrolo[2,1-*c*][1,4]benzodiazepine (PBD) Antitumour Antibiotics, in *Molecular Aspects of Anticancer Drug-DNA Interactions* (Neidle, S., and Waring, M. J., Eds.) pp 54−88, Macmillan, London.
2. Thurston, D. E. (1999) Nucleic Acid Targeting: Therapeutic Strategies for the 21st Century. *Br. J. Cancer 80*, 65–85.
3. Puzanov, I., Lee, W., Berlin, J. D., Calcutt, M. W., Hachey, D. L., Vermeulen, W., Low, J., and Rothenberg, M. L. (2006) Phase I and Pharmacokinetic Trial of SJG-136 Administered on a Daily x 5 Schedule. *EJC Suppl. 4*, 93–93.
4. Hadjivassileva, T., Thurston, D. E., and Taylor, P. W. (2005) Pyrrolobenzodiazepine Dimers: Novel Sequence-Selective, DNA-Interactive, Cross-Linking Agents with Activity against Gram-Positive bacteria. *J. Antimicrob. Chemother. 56*, 513–518.
5. Arora, S. K. (1979) Structural Investigations of Mode of Action of Drugs. 2. Molecular-Structure of Anthramycin Methyl-Ether Monohydrate. *Acta Crystallogr., Sect. B: Struct. Sci. 35*, 2945–2948.
6. Mostad, A., Romming, C., and Storm, B. (1978) Structure of the DNA Complexing Agent Anthramycin. *Acta Chem. Scand., Ser. B 32*, 639–645.

7. Brazhnik, M., Mesentse, A., and Konstant, N. (1972) Sibiromycin—Isolation and Characterization. *J. Antibiot. 25*, 668.
8. Leber, J. D., Hoover, J. R. E., Holden, K. G., Johnson, R. K., and Hecht, S. M. (1988) A Revised Structure for Sibiromycin. *J. Am. Chem. Soc. 110*, 2992–2993.
9. Boyd, F. L., Cheatham, S. F., Remers, W., Hill, G. C., and Hurley, L. H. (1990) Characterization of the Structure of the Anthramycin-d(ATGCAT) $_2$ Adduct by NMR and Molecular Modeling Studies—Determination of the Stereochemistry of the Covalent Linkage Site, Orientation in the Minor Groove of DNA, and Effect on Local DNA-Structure. *J. Am. Chem. Soc. 112*, 3279–3289.
10. Boyd, F. L., Stewart, D., Remers, W. A., Barkley, M. D., and Hurley, L. H. (1990) Characterization of a Unique Tomaymycin-d(CICGAATTCICG) $_2$ Adduct Containing 2 Drug Molecules Per Duplex by NMR, Fluorescence, and Molecular Modeling Studies. *Biochemistry 29*, 2387–2403.
11. Krugh, T. R., Graves, D. E., and Stone, M. P. (1989) 2-Dimensional NMR-Studies on the Anthramycin-d(ATGCAT) $_2$ Adduct. *Biochemistry 28*, 9988–9994.
12. Kopka, M. L., Goodsell, D. S., Baikalov, I., Grzeskowiak, K., Cascio, D., and Dickerson, R. E. (1994) Crystal-Structure of a Covalent DNA Drug Adduct—Anthramycin Bound to C-C-A-A-C-G-T-T-G-G and a Molecular Explanation of Specificity. *Biochemistry 33*, 13593–13610.
13. Rao, S. N., and Remers, W. A. (1990) All Atom Molecular Mechanics Simulations on Covalent Complexes of Anthramycin and Neothramycin with Deoxydecanucleotides. *J. Med. Chem. 33*, 1701–1707.
14. Remers, W. A., Mabilia, M., and Hopfinger, A. J. (1986) Conformations of Complexes between Pyrrolo[1,4]benzodiazepines and DNA Segments. *J. Med. Chem. 29*, 2492–2503.
15. Jones, G. B., Davey, C. L., Jenkins, T. C., Kamal, A., Kneale, G. G., Neidle, S., Webster, G. D., and Thurston, D. E. (1990) The Noncovalent Interaction of Pyrrolo[2,1-*c*][1,4]benzodiazepine-5,11-Diones with DNA. *Anti-Cancer Drug Des. 5*, 249–264.
16. Hertzberg, R. P., Hecht, S. M., Reynolds, V. L., Molineux, I. J., and Hurley, L. H. (1986) DNA-Sequence Specificity of the Pyrrolo[1,4]benzodiazepine Antitumor Antibiotics—Methidium-propyl-EDTA-Iron(II) Footprinting Analysis of DNA-Binding Sites for Anthramycin and Related Drugs. *Biochemistry 25*, 1249–1258.
17. Puvvada, M. S., Forrow, S. A., Hartley, J. A., Stephenson, P., Gibson, I., Jenkins, T. C., and Thurston, D. E. (1997) Inhibition of Bacteriophage T7 RNA Polymerase *In Vitro* Transcription by DNA-Binding Pyrrolo[2,1-*c*][1,4]benzodiazepines. *Biochemistry 36*, 2478–2484.
18. Narayanaswamy, M., Griffiths, W. J., Howard, P. W., and Thurston, D. E. (2008) An Assay Combining High-Performance Liquid Chromatography and Mass Spectrometry to Measure DNA Interstrand Cross-Linking Efficiency in Oligonucleotides of Varying Sequences. *Anal. Biochem. 374*, 173–181.
19. Howard, P. W., Chen, Z., Gregson, S. J., Stephenson, M., Klee, S., Hartley, J., Suggit, M., Loadman, P. M., Evans, D., Hartley, J. A. and Thurston, D. E. (2005) Design, Synthesis and Biological Evaluation of ZC-423, a Novel C2-Aryl Substituted Pyrrolo[2,1-*c*][1,4]benzodiazepine (PBD) dimer, in *Proceedings of the AACR-NCI-EORTC International Conference in Molecular Targets and Cancer Therapeutics*, p 108, AACR, Philadelphia, PA.
20. Cooper, N., Burger, A. M., Matthews, C. S., Howard, P. W., and Thurston, D. E. (2002) Structure-Activity-Relationship (SAR) Study of Novel C2/C3-Unsaturated C2-Aryl-substituted Pyrrolobenzodiazepine Monomer Antitumour Agents. *Eur. J. Cancer 38*, S122–S122.
21. Cooper, N., Hagan, D. R., Tiberghien, A., Ademefun, T., Matthews, C. S., Howard, P. W., and Thurston, D. E. (2002) Synthesis of Novel C2-Aryl Pyrrolobenzodiazepines (PBDs) as Potential Antitumour Agents. *Chem. Commun.,* 1764–1765.
22. Burger, A. M., Loadman, P. M., Thurston, D. E., Schultz, R., Fiebig, H., and Bibby, M. C. (2007) Preclinical Pharmacology of the Pyrrolobenzodiazepine (PBD) Monomer DRH-417 (NSC 709119). *J. Chemother. 19*, 66–78.
23. Antonow, D., Cooper, N., Howard, P. W., and Thurston, D. E. (2007) Parallel Synthesis of a Novel C2-Aryl Pyrrolo[2,1-*c*][1,4]benzodiazepine (PBD) Library. *J. Comb. Chem. 9*, 437–445.
24. Dyong, I., and Schulte, G. (1981) Syntheses of Biologically Important Carbohydrates. 24. Derivatives of Sibirosamine (4,6-Dideoxy-3-C-Methyl-4-Methylamino-D-Altropyranose) by 4-]2 Chirality Transfer and by Vic Cis-Oxyamination of a 3-C-Methyl-Hex-3-Enopyranoside. *Chem. Ber./Recl. 114*, 1484–1502.
25. Hurley, L. H., Gairola, C., and Zmijewski, M. (1977) Pyrrolo(1,4) benzodiazepine Antitumor Antibiotics—In vitro Interaction of Anthramycin, Sibiromycin and Tomaymycin with DNA Using Specifically Radiolabeled Molecules. *Biochim. Biophys. Acta 475*, 521–535.
26. Hwang, T. L., and Shaka, A. J. (1995) Water Suppression That Works—Excitation Sculpting Using Arbitrary Wave-Forms and Pulsed-Field Gradients. *J. Magn. Reson., Ser. A 112*, 275–279.
27. Black, G. D., J., Didier, B., Elsethagen, T., Feller, D., Gracio, D., Hackler, M., Havre, S., Jones, D., Jurrus, E., Keller, T., Lansing, C., Matsumoto, S., Palmer, B., Peterson, M., Schuchardt, K., Stephan, E., Sun, L., Swanson, K., Taylor, H., Thomas, G., Vorpagel, E., Windus, T., and Winters, C. (2006) ECCE, A Problem Solving Environment for Computational Chemistry (Laboratory, P. N. N., Ed.) *Software Version 4.0.2* ed., Richland, WA.
28. Mohamadi, F., Richards, N. G. J., Guida, W. C., Liskamp, R., Lipton, M., Caufield, C., Chang, G., Hendrickson, T., and Still, W. C. (1990) Macromodel—an Integrated Software System for Modeling Organic and Bioorganic Molecules Using Molecular Mechanics. *J. Comput. Chem. 11*, 440–467.
29. Cornell, W. D., Cieplak, P., Bayly, C. I., Gould, I. R., Merz, K. M., Ferguson, D. M., Spellmeyer, D. C., Fox, T., Caldwell, J. W., and Kollman, P. A. (1995) A 2nd Generation Force-Field for the Simulation of Proteins, Nucleic-Acids, and Organic-Molecules. *J. Am. Chem. Soc. 117*, 5179–5197.
30. Still, W. C., Tempczyk, A., Hawley, R. C., and Hendrickson, T. (1990) Semianalytical Treatment of Solvation for Molecular Mechanics and Dynamics. *J. Am. Chem. Soc. 112*, 6127–6129.
31. Chang, G., Guida, W. C., and Still, W. C. (1989) An Internal Coordinate Monte-Carlo Method for Searching Conformational Space. *J. Am. Chem. Soc. 111*, 4379–4386.
32. Shenkin, P. S., and Mcdonald, D. Q. (1994) Cluster-Analysis of Molecular-Conformations. *J. Comput. Chem. 15*, 899–916.
33. Schwieters, C. D., Kuszewski, J. J., and Clore, G. M. (2006) Using XPLOR-NIH for NMR Molecular Structure Determination. *Prog. Nucl. Magn. Reson. Spectrosc. 48*, 47–62.
34. Goodford, P. J. (1985) A Computational-Procedure for Determining Energetically Favorable Binding-Sites on Biologically Important Macromolecules. *J. Med. Chem. 28*, 849–857.
35. Ueda, Y., Kagitani, Y., Sako, E., Suyama, T., Komatsu, N., and Satoh, D. (1979) Benzodiazepines-Processes for producing them and compositions containing them. Patent, Ed., United Kingdom.
36. Kaneko, T., Wong, H., Doyle, T. W., Rose, W. C., and Bradner, W. T. (1985) Bicyclic and Tricyclic Analogs of Anthramycin. *J. Med. Chem. 28*, 388–392.
37. Langlois, N., Rojas-Rousseau, A., Gaspard, C., Werner, G. H., Darro, F., and Kiss, R. (2001) Synthesis and Cytotoxicity on Sensitive and Doxorubicin-Resistant Cell Lines of New Pyrrolo[2,1-*c*][1,4]benzodiazepines Related to Anthramycin. *J. Med. Chem. 44*, 3754–3757.
38. Harris, S. A., Gavathiotis, E., Searle, M. S., Orozco, M., and Laughton, C. A. (2001) Cooperativity in Drug-DNA Recognition: A Molecular Dynamics Study. *J. Am. Chem. Soc. 123*, 12658–12663.
39. Schwieters, C. D., and Clore, G. M. (2001) The VMD-XPLOR Visualization Package for NMR Structure Refinement. *J. Magn. Reson. 149*, 239–244.
40. Puvvada, M. S., Hartley, J. A., Jenkins, T. C., and Thurston, D. E. (1993) A Quantitative Assay to Measure the Relative DNA-Binding Affinity of Pyrrolo[2,1-*c*][1,4]benzodiazepine (PBD) Antitumor Antibiotics Based on the Inhibition of Restriction-Endonuclease Bamhi. *Nucleic Acids Res. 21*, 3671–3675.
41. El Hassan, M. A., and Calladine, C. R. (1998) Two Distinct Modes of Protein-Induced Bending in DNA. *J. Mol. Biol. 282*, 331–343.

BI801225Q